Journal Name

ARTICLE

High-yield synthesis and catalytic response of chainlike hybrid materials of the [$(MoO_3)_m$(2,2'-bipyridine)$_n$] family

Received 00th January 20xx,
Accepted 00th January 20xx

DOI: 10.1039/x0xx00000x

www.rsc.org/

Sofia M. Bruno, Lucie S. Nogueira, Ana C. Gomes, Anabela A. Valente, Isabel S. Gonçalves and Martyn Pillinger*

The one-dimensional organic-inorganic hybrid material [MoO_3(2,2'-bipy)] (**1**) (2,2'-bipy = 2,2'-bipyridine) has been used as a starting material to prepare the bipy-deficient phases [Mo_2O_6(2,2'-bipy)] (**2**) and [Mo_3O_9(2,2'-bipy)$_2$] (**3**) in excellent yields. The hybrid **2** was obtained by a solid-state thermal treatment of **1** (300 °C, 10 min) while **3** was obtained by a hydrothermal treatment of **1** (160 °C, 6 d). A study was performed to compare the catalytic properties of **1**-**3** in the epoxidation of *cis*-cyclooctene at 55 °C with *tert*-butylhydroperoxide (TBHP) or aqueous H_2O_2 as oxidant. In all cases Cy was converted to cyclooctene oxide (CyO) with 100 % selectivity, and Cy conversions increased in the order **1** < **3** < **2**, which parallels an increase in the Mo/2,2'-bipy molar ratio of the hybrid (1 < 1.5 < 2). With compound **2**, CyO yields at 24 h were 96 % for TBHP (cosolvent α,α,α-trifluorotoluene) and 53 % for H_2O_2 (cosolvent CH_3CN). The catalytic reactions occurred in homogeneous phase with active species formed *in situ* from **1**-**3**. All three hybrids react with aqueous H_2O_2 to give the catalytically active oxodiperoxo complex [$MoO(O_2)_2$(2,2'-bipy)]. The 2:1 hybrid **2** was further examined for the epoxidation of other cyclic and linear non-functionalised olefins with TBHP, namely cyclododecene, 1-octene and *trans*-2-octene, and the biomass-derived olefins DL-limonene, α-pinene and methyl oleate.

Introduction

The oxides and oxide-hydrates of molybdenum display a rich variety of structural types and have been extensively studied for applications in catalysis, solar energy conversion, batteries, semiconductors and electronics, amongst others.[1] The thermodynamically stable form of molybdenum trioxide, α-MoO_3, has an orthorhombic structure consisting of distorted {MoO_6} octahedra that share edges and corners to form two-dimensional (2D) MoO_3 sheets separated in the lattice by van der Waals gaps.[1] The unique layered structure of α-MoO_3 permits topotactic redox chemistry involving the intercalation of small ions (e.g. alkali metal cations and H^+) and a partial reduction of the Mo oxidation state.[2] Protons intercalate to give hydrogen molybdenum bronzes (HMB) H_xMoO_3 ($0 < x \leq 2$) with metallic features and molybdenum/oxygen frameworks that are almost unchanged as compared to the host lattice MoO_3.[3] HMB can react further in a topotactic fashion with Lewis bases (L) such as pyridine (py) to give the layered intercalation compound $py_{0.3}H_{0.5}MoO_3$.[4] On the other hand, when excess pyridine is heated with α-MoO_3 under anhydrous conditions, the structure of the MoO_3 layers completely changes and a different phase is obtained ([MoO_3(py)]) in which {MoO_5N} octahedra share corners with four other octahedra to form infinite molybdenum oxide sheets with alternate apical arrangements of Mo–N(py) and Mo=O.[5] Performing the intercalation reaction with 4,4'-bipyridine led to the compound formulated as [MoO_3(4,4'-bipy)$_{0.5}$] which was proposed to possess an analogous structure with the difference that the organic ligand acts as a pillar cross-linking adjacent layers.[5]

The compounds [MoO_3(py)] and [MoO_3(4,4'-bipy)$_{0.5}$] were the first members of a class of hybrid materials that have been termed metal oxide-organic frameworks or coordination polymers.[6] These compounds are distinguished by having an extended metal oxide component decorated by organic ligands (frequently an organoamine or organocarboxylate). The organic ligands play a critical role in dictating the inorganic oxide substructure. The original syntheses of [MoO_3(py)] and [MoO_3(4,4'-bipy)$_{0.5}$] were tedious, involving long reaction times of two to four weeks, elevated temperatures (160-250 °C), and intermediate regrinding of the solid phase.[5] In later years the techniques of hydrothermal synthesis were found to be much more effective for the isolation of novel hybrid materials based on metal oxides. Zubieta and coworkers confirmed the structure of [MoO_3(4,4'-bipy)$_{0.5}$] by isolating single-crystals of the compound through the hydrothermal reaction of MoO_3 with 4,4'-bipy at 150 °C.[7] The layered perovskite-like motif found in this compound and in [MoO_3(py)] has also been identified in the tungsten isostructures[8] and in the hybrid materials [MO_3(pyrazine)$_{0.5}$] (M = Mo, W),[8,9] [WO_3(1,2-bipyridylethane)],[8a] [MO_3(trz)$_{0.5}$] (M = Mo, W; trz = 1,2,3-triazole or 1,2,4-triazole),[7,10] and [MoO_3(3,8-phenanthroline)$_{0.5}$].[11]

Department of Chemistry, CICECO - Aveiro Institute of Materials, University of Aveiro, Campus Universitário de Santiago, 3810-193 Aveiro, Portugal. E-mail: mpillinger@ua.pt (M. Pillinger)

† Electronic Supplementary Information (ESI) available: PXRD patterns, ATR FT-IR spectra and Raman spectra of **1**-**5** and recovered catalysts, variable temperature PXRD data for **2** and **3**, and miscellaneous catalytic data (contact tests, cyclooctene epoxidation with H_2O_2, and ethanolysis of styrene oxide). See DOI: 10.1039/x0xx00000x

Chelating ligands such as 2,2'-bipy tend to restrict the oxide dimensionality to chains or ribbons since their coordination blocks at least two condensation sites on the same metal center.[12,13] In the case of 2,2'-bipy, a hydrothermal synthesis led to the compound [MoO_3(2,2'-bipy)], which has a structure consisting of 1D chains of corner-sharing distorted {MoO_4N_2} octahedra.[13a] By variation of the synthesis conditions, derivatives of this 1D polymer have been obtained in which the repeat unit consists of one {MoO_4} tetrahedron and either one, two or three {MoO_4N_2} octahedra.[13a,13c]

Hydrothermal methods for the preparation of molybdenum oxide-organoamine hybrid materials suffer from common problems such as low yields and the formation of mixtures that must be mechanically separated. We have been exploring alternative approaches involving the use of metallo-organic complexes as synthesis precursors.[14] The oxidative decarbonylation of molybdenum carbonyl complexes under mild conditions has proved to be a particularly useful technique and, in the case of the tetracarbonyl complex *cis*-[$Mo(CO)_4$(2,2'-bipy)], allowed the isolation of [MoO_3(2,2'-bipy)] (**1**) in near-quantitative yield.[14a] Polymeric **1** has given interesting results as a catalyst for the epoxidation of olefins,[14a] the oxidation of secondary amines to nitrones,[15] and the oxidation of sulfides to sulfoxides or sulfones.[15] The existence of the bipy-deficient derivatives of **1** provides a potential avenue for systematically studying structure-performance relationships with respect to the use of the compounds in catalysis. With this in mind, we sought improved syntheses of these hybrid materials to make them readily available for catalytic investigations. The synthetic advances reported herein comprise the use of polymeric **1** as a starting material to prepare [Mo_2O_6(2,2'-bipy)] (**2**) (by a solid-state thermal transformation) and [Mo_3O_9(2,2'-bipy)$_2$] (**3**) (by a hydrothermal reaction). A comparative study has been performed on the catalytic performances of **1**-**3** in the epoxidation of *cis*-cyclooctene.

Experimental Section

Materials and methods

MoO_3 (99.5%, Analar, BDH Chemicals), 2,2'-bipyridine, 5.0-6.0 M *tert*-butylhydroperoxide in decane, 30 wt.% hydrogen peroxide, dichloromethane (puriss grade), diethyl ether (99.8 %), acetone (99.5 %), hexane (≥ 95 %, Carlo Erba), pentane (≥ 95%, Carlo Erba), α,α,α-trifluorotoluene (> 99 %), acetonitrile (≥ 99.9 %), *cis*-cyclooctene (Alfa Aesar, 95 %), 1-octene (97 %), *trans*-2-octene (97 %), cyclododecene (mixture of *cis* and *trans* isomers, 96 %), DL-limonene (≥ 95 %, Merck), α-pinene (98 %), and methyl oleate (99 %) were purchased from Sigma-Aldrich unless otherwise indicated, and used as received. The 1D polymeric material [MoO_3(2,2'-bipy)] (**1**) was obtained in 97 % yield as described previously by oxidative decarbonylation of *cis*-[$Mo(CO)_4$(2,2'-bipy)] with *tert*-butylhydroperoxide (TBHP).[14a] The [MoO_3(2,2'-bipy)]/molybdenum oxide hybrid material {[MoO_3(2,2'-bipy)][$MoO_3(H_2O)$]}$_n$ (**4**) was prepared by treatment of [MoO_2Cl_2(2,2'-bipy)][16] with water under reflux.[14b]

Microanalyses for C, H and N were carried out at the Department of Chemistry, University of Aveiro, with a Truspec Micro CHNS 630-200-200 elemental analyser. Thermogravimetric analysis (TGA) was performed using a Shimadzu TGA-50 system at a heating rate of 5 °C min^{-1} under air. Powder X-ray diffraction (PXRD) data were collected at ambient temperature using a PANalytical Empyrean instrument equipped with a PIXcel 1D detector set at 240 mm from the sample. Cu-K$\alpha_{1,2}$ X-radiation (λ_1 = 1.540598 Å; λ_2 = 1.544426 Å) filtered with a nickel foil was used along with a standard transmission sample holder. Working operating conditions for the X-ray tube: 45 kV and 40 mA. Intensity data were collected in continuous mode in the ca. $3.0 \le 2\theta \le 70.0°$ range. Variable temperature PXRD was carried out using a PANalytical X'Pert PRO3 HTK 16N high temperature chamber containing a Pt heating filament and a Pt-Pt/Rh (10%) thermocouple. The powdered sample was deposited on a Pt sheet which was then placed over the heating element. Heating rates of 5 °C min^{-1} were used. At a given temperature, samples were step-scanned in 0.02° 2θ steps with a counting time of 200 s per step. Transmission FT-IR spectra were measured on a Mattson 7000 spectrometer (128 scans and resolution of 4.0 cm^{-1}) in the 300–4000 cm^{-1} range using KBr pellets. Attenuated total reflectance (ATR) FT-IR spectra were recorded on the same instrument equipped with a Specac Golden Gate Mk II ATR accessory having a diamond top-plate and KRS-5 focussing lenses (256 scans and resolution of 4.0 cm^{-1}). FT-Raman spectra were recorded on a RFS-100 Bruker FT-Spectrometer equipped with a Nd:YAG laser with an excitation wavelength of 1064 nm. $^{13}C\{^1H\}$ CP MAS NMR spectra were recorded using a Bruker Avance 400 (narrow bore) spectrometer with an ultrashielded static magnetic field of 100.6 MHz. The spectra were recorded with 2.75 μs ^{1}H 90° pulses, 2.0 ms contact time, spinning rate of 14 kHz, and 5 s recycle delays. Chemical shifts are quoted in ppm from TMS.

Syntheses

[Mo_2O_6(2,2'-bipy)] (2). [MoO_3(2,2'-bipy)] (**1**) (21 mg, 0.07 mmol) was heated under air for 10 min in a muffle furnace preheated to 300 °C. Yield: 15 mg, 96%. Anal. Calcd for $C_{10}H_8Mo_2N_2O_6$ (444.06): C, 27.05; H, 1.82; N, 6.30. Found: C, 26.80; H, 1.87; N, 6.00 %. FT-IR (KBr, cm^{-1}): 308 (m), 324 (m), 355 (m), 380 (m), 704 (vs), 771 (vs), 883 (vs), 903 (vs), 919 (sh), 941 (s), 960 (m), 1003 (w), 1028 (m), 1062 (w), 1101 (w), 1157 (w), 1180 (w), 1221 (w), 1243 (w), 1284 (w), 1320 (m), 1425 (m), 1444 (s), 1473 (m), 1493 (m), 1574 (m), 1598 (s), 1606 (sh), 3058 (w), 3105 (w), 3420 (br). Selected FT-Raman (cm^{-1}): 895 (w), 936 (m), 969 (w), 1025 (w), 1308 (w), 1564 (w), 1595 (m), 3073 (w). $^{13}C\{^1H\}$ CP MAS NMR: δ= 152.3 (C2/C2'), 149.5 (C2/C2', C6/C6'), 144.9, 142.0 (C4/C4'), 128.4 (C5/C5'), 126.1 (C5/C5', C3/C3'), 124.4 (C3/C3').

[Mo_3O_9(2,2'-bipy)$_2$] (3). A mixture of [MoO_3(2,2'-bipy)] (**1**) (0.20 g, 0.67 mmol) and H_2O (25 mL) was heated under autogenous pressure and dynamic conditions (25 rpm) for 6 d at 160 °C in a Teflon-lined stainless-steel digestion bomb. The resultant solid was filtered, washed with water (3 × 5 mL), acetone (3 × 5 mL)

and diethyl ether (2 × 5 mL), and finally vacuum-dried. Yield: 0.14 g, 85 %. Anal. Calcd for $C_{20}H_{16}Mo_3N_4O_9$ (744.18): C, 32.28; H, 2.17; N, 7.53. Found: C, 32.10; H, 2.17; N, 7.30%. FT-IR (KBr, cm^{-1}): 301 (w), 316 (w), 332 (m), 386 (m), 420 (w), 442 (w), 635 (sh), 649 (vs), 665 (vs), 742 (s), 758 (s), 775 (vs), 798 (vs), 897 (vs), 914 (vs), 938 (s), 1026 (m), 1161 (w), 1176 (w), 1227 (w), 1248 (w), 1315 (m), 1442 (s), 1473 (m), 1493 (m), 1574 (w), 1597 (s), 3035 (w), 3076 (w), 3105 (w), 3438 (br). FT-Raman (cm^{-1}): 106 (w), 124 (w), 154 (w), 188 (w), 198 (w), 222 (w), 236 (w), 249 (w), 259 (w), 301 (w), 315 (w), 338 (w), 355 (w), 383 (w), 634 (w), 652 (w), 767 (w), 779 (w), 800 (w), 814 (w), 830 (w), 870 (w), 896 (m), 925 (vs), 948 (m), 1024 (s), 1061 (w) 1164 (w), 1269 (w), 1288 (vw), 1316 (vs), 1494 (m), 1565 (s), 1597 (vs), 2984 (w), 3078 (m), 3131 (w). $^{13}C\{^1H\}$ CP MAS NMR: δ = 153.1, 150.5 (C2/C2'), 148.8, 147.8 (C6/C6'), 143.5, 141.6, 138.9 (C4/C4'), 128.8 (sh), 128.4, 127.3, 125.5 (C5/C5'), 125.0 (sh), 123.2, 122.8 (sh), 120.7 (C3/C3').

[$MoO(O_2)_2$(2,2'-bipy)] (5). A mixture of MoO_3 (0.25 g, 1.73 mmol) and 30 % H_2O_2 (2.50 mL, 24.5 mmol) was stirred for 3 h at 60 °C under N_2. The resultant yellow solution was cooled in an ice-bath and then 2,2'-bipy (0.27 g, 1.73 mmol) was added slowly. A yellow paste was obtained at this stage. After decanting off the supernatant, the residue was washed with H_2O (3 × 10 mL), pentane (4 × 10 mL) and diethyl ether (2 × 10 mL), obtaining a yellow solid, which was finally vacuum-dried. Yield: 0.43 g, 75 %. FT-IR and Raman spectral data for **5** were in agreement with those reported previously.[17]

Catalytic tests

The catalytic reactions were carried out in magnetically stirred, closed borosilicate reaction vessels (10 mL capacity) which were immersed in an oil bath set to 55 °C. For the epoxidation reaction, the reactor was loaded with molybdenum complex (18 µmol), *cis*-cyclooctene (1.8 mmol), oxidant (TBHP or H_2O_2, 2.75 mmol) and solvent (1 mL α,α,α-trifluorotoluene or CH_3CN). The solvent and catalyst were pre-heated at the reaction temperature for 10 min prior to addition of the reactants (instant taken as zero time). The course of the reaction was monitored using a Varian 3800 GC equipped with a Bruker BR-5 capillary column (30 m × 0.25 mm; 0.25 µm) and a flame ionisation detector, using H_2 as the carrier gas. Undecane was used as an internal standard added after the reaction. The products were identified by GC-MS (Trace GC 2000 Series (Thermo Quest CE Instruments) - DSQ II (Thermo Scientific)), equipped with an Agilent J&W capillary DB-5 column (30 m × 0.25 mm; 0.25 µm) and using He as carrier gas.

After the catalytic reaction, the catalysts were separated from the reaction mixtures by centrifugation, thoroughly washed with pentane and dried under reduced pressure (ca. 1 mbar) for 1 h at 60 °C. The recovered catalysts (**i**-Cat-ox, where **i** is the compound number and ox is the oxidant) were characterised by ATR FT-IR spectroscopy and PXRD.

Contact tests (CTs) were carried out by mixing the original catalyst with oxidant and solvent (without substrate) and stirring for 24 h at 55 °C. Subsequently the solid phase was separated by centrifugation, and the supernant (L) was filtered through a 0.22 µm PTFE membrane, giving the solution denoted **i**-CT-ox-L. The solid (S) was washed with pentane and dried under reduced pressure for 1 h at 60 °C, giving **i**-CT-ox-S. These solids were characterised by ATR FT-IR spectroscopy and PXRD, and tested for the Cy reaction under similar conditions to those used for the original catalysts. The liquid phase **i**-CT-ox-L was transferred to a new reactor, and pre-heated to 55 °C for 10 min. Subsequently, the pre-heated substrate was added to the reactor in an amount to give the same initial molar concentration of Cy as that used for a normal catalytic run.

The oxidant efficiency was determined by iodometric titration of the reaction mixtures, after a 24 h batch run at 55 °C. The values indicated in the discussion are the average of three replicates (range of experimental error was ca. 10 %). The catalyst acidity tests were carried out as described in the ESI† using styrene oxide as substrate.

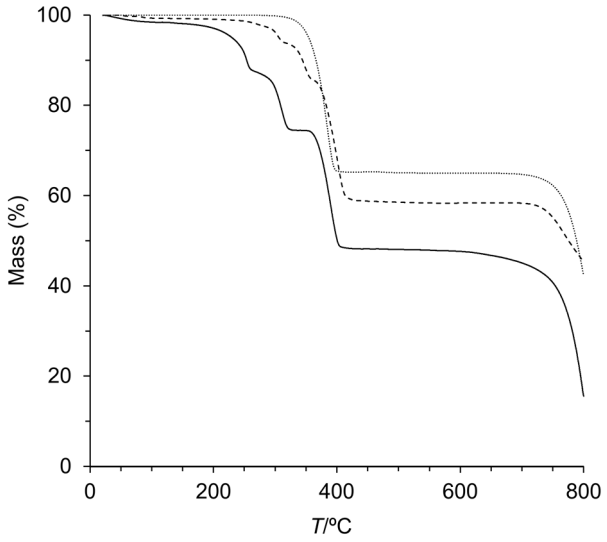

Fig. 1 TGA curves for compounds **1** (——), **2** (·····) and **3** (– – –).

Results and Discussion

Thermal stability studies and polymer syntheses

Thermogravimetric analysis (TGA) of [MoO_3(2,2'-bipy)] (**1**) under air shows a mass loss of 48.8 % in the interval 200-425 °C, divided into three sequential steps, corresponding to the decomposition of 2,2'-bipy moieties (Fig. 1). No further weight loss takes place until 625 °C. The residual mass of 48.3 % at 425 °C is in very good agreement with the calculated value of 48.0 % assuming that full decomposition of the organic ligands leads to MoO_3. This was confirmed by performing a variable temperature PXRD experiment (Fig. 2). The results show that reflections characteristic of microcrystalline **1** are present up to 320 °C, although a slight loss of crystallinity is apparent when comparing the pattern obtained at this temperature (Fig. 2b) with that obtained for **1** at ambient temperature (Fig. 2a). Further heating to 350 °C (Fig. 2c) leads to complete loss of reflections due to **1** and the appearance of a new phase with reflections that match those present in the simulated PXRD pattern for the 1D polymeric material [Mo_2O_6(2,2'-bipy)] (**2**)

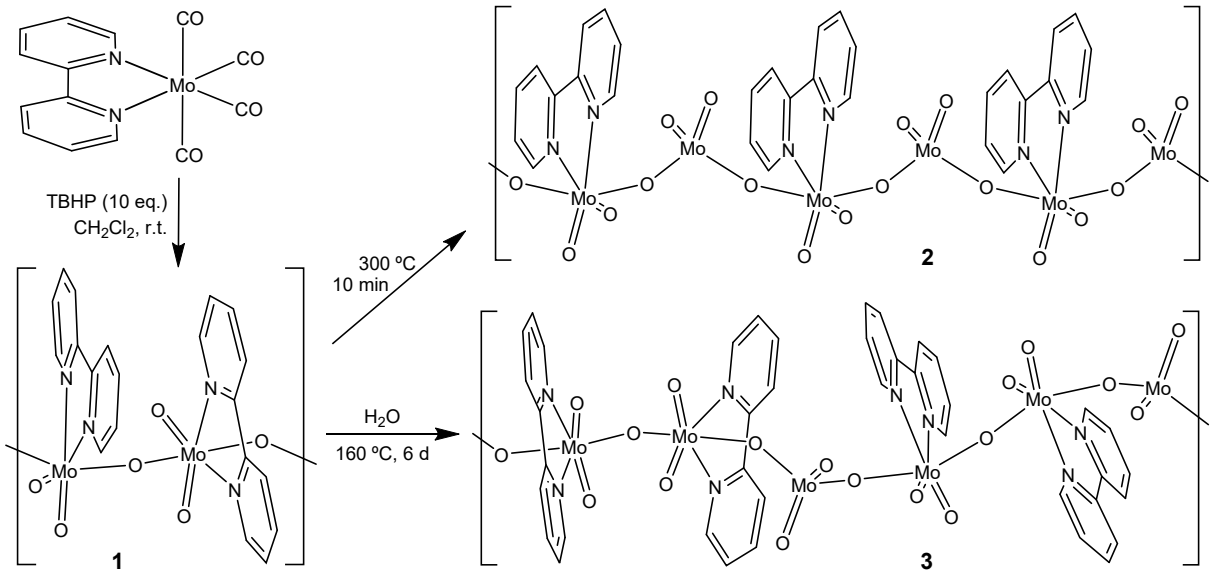

Scheme 1 Synthesis of compounds **1**-**3**.

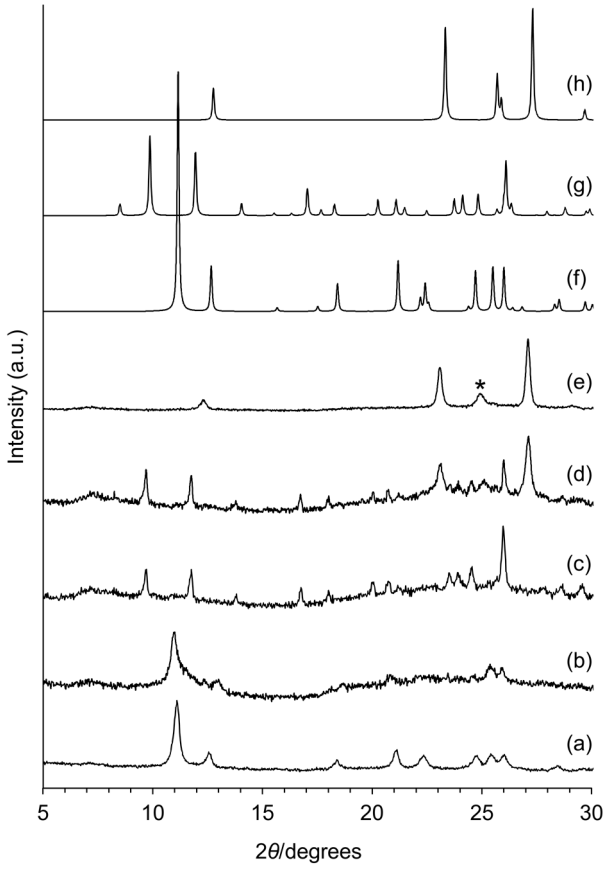

Fig. 2 Variable temperature PXRD study of $[MoO_3(2,2'\text{-bipy})]$ (**1**): (a) ambient temperature, (b) 320 °C, (c) 350 °C, (d) 420 °C, (e) 570 °C. The computed patterns for **1** (f), $[Mo_2O_6(2,2'\text{-bipy})]$ (**2**) (g) and α-MoO_3 (h) were generated using the program Mercury (copyright CCDC, ver. 3.9)[18] with crystallographic data published for **1**/**2**[13a] and α-MoO_3.[19] The asterisk in pattern (e) identifies an unassigned reflection; all other reflections are due to α-MoO_3.

(Fig. 2g). Accordingly, the residual mass of 74.4 % at 350 °C in the TGA profile of **1** (*i.e.*, the mass registered at the well-defined plateau observed after the second of three sequential weight loss steps) is in excellent agreement with the calculated value of 74.0 % assuming complete conversion of **1** to **2** with the loss of 0.5 equiv. of 2,2'-bipy. In line with the TGA profile, the *in situ* PXRD study shows that the intermediate phase **2** only persists over a narrow temperature range since the pattern recorded at 420 °C (Fig. 2d) contains peaks characteristic of orthorhombic α-MoO_3 (Fig. 2h). The PXRD pattern recorded at 570 °C (Fig. 2e) shows loss of all reflections due to **2**. Sublimation of molybdenum oxide occurs above 625 °C (Fig. 1). These results for the thermal behaviour of **1** are in agreement with the *in situ* Raman study reported by Twu *et al.*[20]

The thermal behaviour of **1** suggests that it could be used as a starting material for the synthesis of **2** via a carefully controlled thermal treatment in the solid-state. A new high-yield synthesis of **2** is desirable since the hydrothermal method reported by Zubieta and coworkers, consisting of heating a mixture of Na_2MoO_4, MoO_3, 2,2'-bipy, $MnCl_2$ and H_2O for 4 days at 200 °C, only led to a 10 % yield of **2** (based on molybdenum) as single-crystals (colourless plates).[13a] In their *in situ* Raman study, Twu *et al.* found that heating **1** to 330 °C gave **2**, but that cooling of this sample to ambient temperature led to the appearance of additional phases identified as MoO_3 and $[Mo_3O_9(2,2'\text{-bipy})_2]$ (**3**).[20] We optimised the thermal treatment of **1** and found that pure **2** could be prepared in quantitative yield by heating **1** at 300 °C for 10 min in a muffle furnace, which constitutes a clean and efficient protocol (Scheme 1). The PXRD pattern of the resultant solid cooled to ambient temperature matched the simulated pattern calculated using the crystal structure data published for **2**,[13a] and did not display reflections due to MoO_3 and/or **3** (Fig. S1 in the ESI†).

The Raman spectrum of **2** displays bands at 895 [ν_{asym}(Mo=O)] and 936 cm^{-1} [ν_{sym}(Mo=O)], which concord with the bands reported by Twu *et al.* (Fig. S2 in the ESI†).[20] Four ν(Mo=O) bands are observed in the FT-IR spectrum at 883, 903, 919 and 941 cm^{-1} (Fig. 3c). A very strong, broad band at 704 cm^{-}

[1] is assigned as a Mo–O–Mo asymmetric stretching vibration. The corresponding band for **1** is centred around 640 cm^{-1}. Regarding the internal 2,2'-bipy vibrational modes, the strong band at 771 cm^{-1} is due to a CH out-of-plane bending vibration (cf. 756 cm^{-1} for free 2,2'-bipy in the solid-state). The shift of the ring stretching bands from ca. 1556 and 1572 cm^{-1} for the free ligand to 1574 and 1598/1606 cm^{-1} for **2** is a direct consequence of bidentate coordination of 2,2'-bipy to the Mo^{VI} centres. It is noteworthy that the spectra of **1** (Fig. 3b) and **2** (Fig. 3c) are very similar in the 1000-1620 cm^{-1} region containing ligand-centred modes. The $^{13}C\{^1H\}$ CP MAS NMR spectra of **1** and **2** display between seven and eight resolved peaks, some of which clearly comprise overlapping resonances (Fig. 4). These spectra are therefore consistent with the reported crystal structures which show that each polymer contains one crystallographically distinct 2,2'-bipy moiety, with the carbon atoms of each Cn/Cn' pair being crystallographically inequivalent.

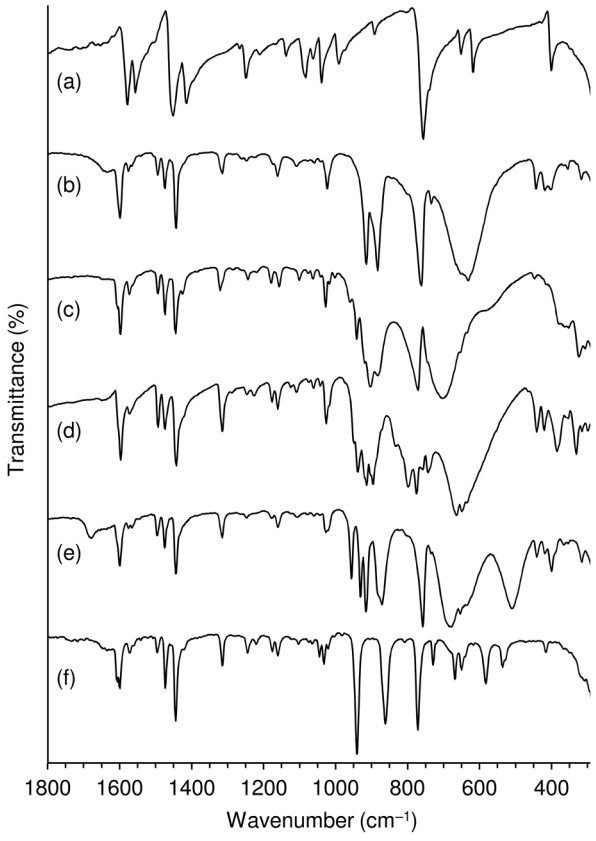

Fig. 3 FT-IR (KBr) spectra in the range of 300-1800 cm^{-1} for (a) 2,2'-bipy, (b) **1**, (c) **2**, (d) **3**, (e) **4** and (f) **5**.

TGA of the polymer **2** shows that decompositions starts above 350 °C (DTG_{max} = 385 °C; DTG = derivative thermogravimetric) (Fig. 1). An *in situ* PXRD study confirmed that the compound is stable at 285 °C, while the pattern recorded at 420 °C corresponds to MoO_3 (Fig. S3 in the ESI†). These data are consistent with the thermal behaviour of **1** above 300 °C, *i.e.* after partial loss of 2,2'-bipy moieties to give the intermediate phase **2**.

The polymer formulated as $[Mo_3O_9(2,2'\text{-bipy})_2]$ (**3**) was the third member of the series $[(MoO_3)_m(2,2'\text{-bipy})_n]$ described by Zubieta and coworkers.[13a] The repeat unit of the 1D polymer chain in **3** consists of one $\{MoO_4\}$ tetrahedron and two $\{MoO_4N_2\}$ octahedra (Scheme 1), as opposed to one $\{MoO_4\}$ tetrahedron and one $\{MoO_4N_2\}$ octahedron in **2**. Our attempts to prepare **3** by the literature method,[13a] consisting of the hydrothermal treatment of a mixture of MoO_3, 2,2'-bipy and H_2O at 160 °C for 6 days (under both static and dynamic conditions), were unsuccessful, leading to mixtures of **3** and other unidentified phases. A successful synthesis of **3** in 85 % yield was subsequently achieved by the hydrothermal treatment of $[MoO_3(2,2'\text{-bipy})]$ (**1**) in H_2O at 160 °C for 6 days. Phase purity was confirmed by PXRD (Fig. S1 in the ESI†).

The vibrational spectra of **3** display several Mo=O stretching bands in the region 880-950 cm^{-1}. According to Twu *et al.*, the Raman bands at 896, 925, and 948 (Fig. S2 in the ESI†) can be ascribed to ν_{asym}(Mo=O) of MoO_4N_2 octahedra, ν_{sym}(Mo=O) of MoO_4N_2 octahedra, and ν_{sym}(Mo=O) of MoO_4 tetrahedra, respectively.[20] Three ν(Mo=O) bands (with additional shoulders) are observed in the FT-IR spectrum at 897, 914 and 938 cm^{-1} (Fig. 3d). Strong, overlapping bands for ν_{asym}(Mo–O–Mo) are observed at 649 and 665 cm^{-1}, *i.e.* at intermediate frequencies when compared with the corresponding bands for **1** and **2**. The spectrum in the region containing ligand-centred modes (1000-1620 cm^{-1}) is very similar to those for **1** and **2**. According to the crystal structure reported for **3**,[13a] the asymmetric unit contains two nonequivalent 2,2'-bipy moieties, with the carbon atoms of each Cn/Cn' pair being crystallographically inequivalent. The $^{13}C\{^1H\}$ CP MAS NMR spectrum of **3** is consistent with this structure since at least sixteen peaks/shoulders can be observed in the aromatic region (114-155 ppm) (Fig. 4d).

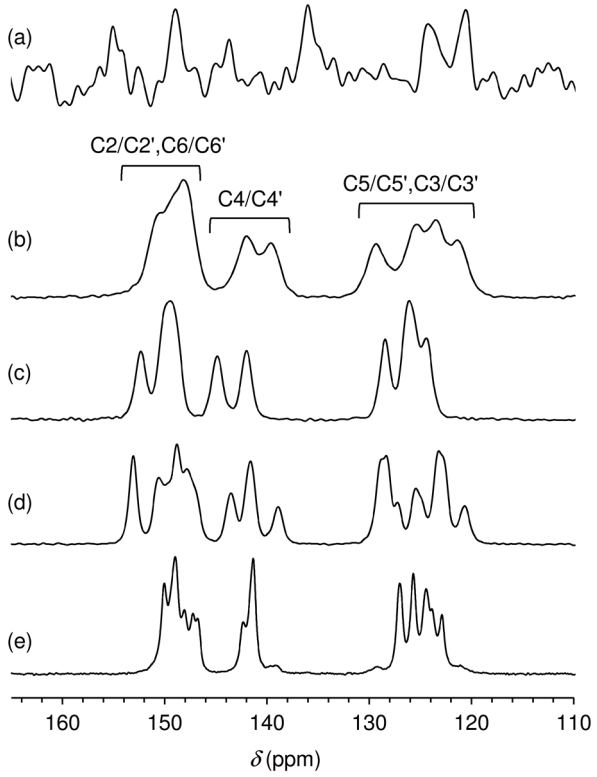

Fig. 4 $^{13}C\{^1H\}$ CP MAS NMR spectra for (a) 2,2'-bipy, (b) **1**, (c) **2**, (d) **3** and (e) **4**.

The thermal decomposition behaviour of **3** was examined by TGA (Fig. 1) and *in situ* PXRD (Fig. S4 in the ESI†). The compound is stable up to 250 °C. The PXRD pattern recorded at this temperature is similar to that for **3** at ambient temperature, although a general shift of reflections towards lower angles took place upon heating. A further shift of the high-angle peaks towards lower angles is evident upon increasing the temperature to 280 °C, while the relative intensity of low-angle peaks around 11° 2θ decreases significantly, which can be associated with the onset of thermal removal of the organic ligands. Loss of 2,2'-bipy moieties takes place in three sequential steps up to 425 °C with DTG_{max} at 305, 348 and 402 °C. The PXRD recorded at 315 °C, *i.e.* after the first weight loss step (3.7 % mass loss between 280 and 315 °C), shows complete loss of reflections below 15° 2θ, while higher-angle reflections are retained, albeit with a further shift towards lower angles. These results suggest that the 1D polymeric chain structure may be retained up to 315 °C despite partial loss of organic ligands. Some of the high-angle reflections persist even after the second weight loss step up to 360 °C. A residual mass of 58.8 % is obtained at 450 °C after complete 2,2'-bipy decomposition, which is close to the calculated value of 58.0 % for MoO_3. However, unlike **1** and **2**, PXRD did not show the formation of a crystalline α-MoO_3 phase between 450 and 700 °C.

Catalytic studies

The polymeric compounds **2** and **3** were investigated for the liquid-phase epoxidation of *cis*-cyclooctene (Cy) using TBHP as oxidant, α,α,α-trifluorotoluene (TFT) as cosolvent, and a reaction temperature of 55 °C. For comparison, the MoO_3/bipyridine hybrid compounds **1** and $\{[MoO_3(2,2'\text{-bipy})][MoO_3(H_2O)]\}_n$ (**4**) were tested under identical Cy reaction conditions. Commercial MoO_3 and the mononuclear complex $[MoO(O_2)_2(2,2'\text{-bipy})]$ (**5**) were chosen for catalyst benchmarking. In all cases Cy was converted to cyclooctene oxide (CyO) with 100 % selectivity (Fig. 5). The reaction without catalyst gave 6 % conversion at 24 h. Based on mechanistic studies reported in the literature for Mo-catalysed olefin epoxidation with hydroperoxide oxidants, a Lewis acid-base reaction (heterolytic mechanism) is generally involved in the formation of an active oxidising species. Specifically, the coordination reaction between the metal centre (Lewis acid) and the oxidant TBHP (Lewis base) leads to an active oxidising species responsible for O-atom transfer to the olefin, giving the respective epoxide product.[16,21] The Lewis acidity of **1**-**4** was assessed via the model reaction of the acid-catalysed ethanolysis of styrene oxide (ESI†). The four compounds led to 2-ethoxy-2-phenylethanol as the only product, at 70-100 % conversion, at 24 h, 55 °C (Table S1). Compounds **5** and MoO_3 were also effective for the acid-catalysed reaction (Table S1), and thus may act as Lewis acids in a similar fashion to **1**-**4**.

The Cy reaction mixtures in the presence of **1**-**5** and MoO_3 were biphasic solid-liquid (S-L). To check for a possible homogeneous phase catalytic contribution, contact tests (CTs) were performed in which each compound was treated with oxidant and cosolvent (but no Cy) for 24 h at 55 °C. The resultant liquid phases, denoted **i**-CT-TBHP-L (**i** = **1**-**5** or MoO_3), were tested for Cy reaction, and led to significant conversions (Fig. S8 in the ESI†). Hence, the catalytic reactions in the presence of the studied molybdenum compounds occurred in homogeneous phase. The kinetic differences between the homogenous catalytic reaction using **i**-CT-TBHP-L and the original catalyst **i** may be partly due to differences in the amount of active species (in contrast to the CTs, in the normal catalytic tests the olefin is present from the initial instant, which may influence the polarity of the medium and catalyst solubility). The solids **i**-CT-TBHP-S (**i** = **1**-**4**) recovered from the CTs were effective for Cy epoxidation, and the kinetic profiles were roughly coincident with those for the respective as-synthesised catalysts (Fig. S8a-d). For MoO_3 and **5**, differences in reaction kinetics were verified in relation to the respective solids MoO_3-CT-TBHP-S and **5**-CT-TBHP-S (Fig. S8e,f).

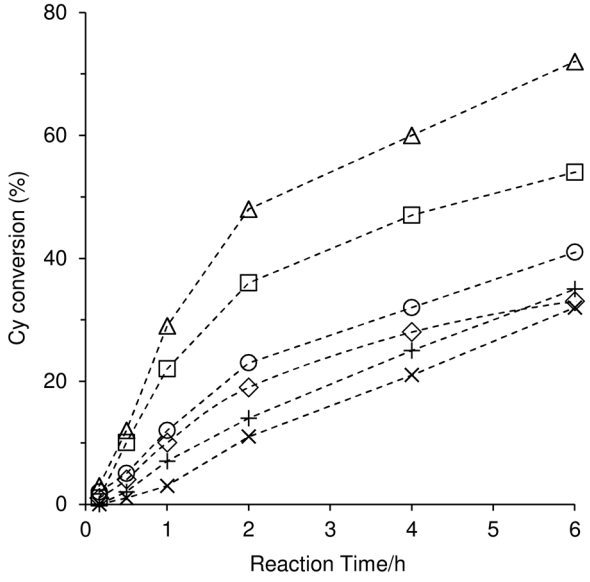

Fig. 5 Kinetic profiles of the catalytic epoxidation of Cy with TBHP, in the presence of **1** (○), **2** (Δ), **3** (□), **4** (◊), **5** (+), and MoO_3 (×), at 55 °C.

Based on the amount of dissolved compound, the initial turnover frequencies for Cy epoxidation (TOF, mol mol_{Mo}^{-1} h^{-1}) were calculated, and increased in the order **5** (42) < MoO_3 (75) < **3** (147) < **1** (200) < **4** (248) < **2** (288). On the other hand, Cy conversion (%) at 24 h increased in the order **4** (62) < **1** (71) < MoO_3 (77) ≈ **3** (78) < **5** (90) < **2** (96). Hence, **2** possessed the highest initial activity, and led to the highest Cy conversion at 24 h. Based on these results and literature data for **1** and **4** tested for Cy/TBHP (with DCE as cosolvent),[14a,b] the two compounds performed worse than **2**. Several other polynuclear or polymeric oxomolybdenum compounds have been tested for this specific reaction using comparable catalytic conditions (Table 1). Higher Cy conversions were reported for $[Mo_2O_6(di\text{-}t\text{Bu-bipy})_2]$,[23] $[Mo_8O_{24}(pzpyEA)_4]$,[24] and $[Mo_2O_6(pent\text{-}pzpy)]$.[25]

The oxidant efficiency for the molybdenum catalysts is an important factor for sustainable catalytic epoxidation processes. Iodometric titrations indicated very high or excellent TBHP efficiencies of 92-100 % for the molybdenum catalysts tested (Fig. S9 in the ESI†).

The catalytic performances of **1**-**4** were further studied using H_2O_2 as oxidant instead of TBHP, and keeping the remaining reaction conditions constant. The Cy/H_2O_2 reaction in the presence of **1**-**4** led to poor results (< 5 % conversion at 24 h), which may be partly due to mass transfer limitations since these systems consisted of triphasic solid-liquid(aqueous)-liquid(organic) mixtures. Changing the cosolvent from TFT to CH_3CN led to biphasic solid-liquid mixtures, and the catalytic results improved (Fig. S10 in the ESI†): conversion (%) at 24 h increased in the order **1** (16) < **3** (31) < **4** (53) = **2** (53). The kinetic profiles for (**1**-**4**)/H_2O_2/CH_3CN were intermediate between those for **5** (21 % conversion at 24 h) and MoO_3 (74 % conversion at 24 h). In general, the H_2O_2 efficiencies were high (97-100 %), with MoO_3 leading to the lowest efficiency (91 %) (Fig. S9).

Table 1 Comparison of the catalytic results for **2** for Cy epoxidation with TBHP with literature data for organo-oxomolybdenum compounds containing a bidentate *N*,*N*-ligand coordinated Mo centers.[a]

Compound[b]	Solvent/*T*(°C)[c]	Time (h)	Conv. (%)[d]	Ref.
2	TFT/55	6/24	72/96	This work
1	DCE/55	6/24	48/81	14a
4	DCE/55	24	45	14b
5	$[C_8mim]PF_6$/60	12	10	22
$[Mo_2O_6(di\text{-}tBu\text{-}bipy)_2]$	ws/55	6/24	93/100	23
$[Mo_8O_{24}(di\text{-}tBu\text{-}bipy)_4]$	DCE/55	6/24	65/90	14a
$[Mo_3O_9(pzpy)]$[e]	ws/55	6/24	29/51	14c
$[Mo_4O_{12}(pzpy)_4]$	ws/55	6/24	55/92	24
$[Mo_2O_6(pent\text{-}pzpy)]$[e]	DCE/55[f]	6	99	25
$[MoO(O_2)_2(pzpyEA)]$	TFT/55[g]	6/24	~10/~20	26
$[Mo_8O_{24}(pzpyEA)_4]$	ws/55	6/24	89/100	24
$[MoO_3(pbim)]$	TFT/55	6/24	30/56	27
$[MoO(O_2)_2(pbim)]$	TFT/70	6/24	81/98	27

[a] Reaction conditions (unless otherwise specified): Mo:Cy:TBHP = 1:100:150. [b] di-*t*Bu-bipy = 4,4'-di-*tert*-butyl-2,2'-bipyridine, pzpy = 2-[3(5)-pyrazolyl]pyridine, pent-pzpy = 2-(1-pentyl-3-pyrazolyl)pyridine, pzpyEA = (ethyl[3-(pyridin-2-yl)-1H-pyrazol-1-yl]acetate), pbim = 2-(2-pyridyl)-benzimidazole. [c] DCE = 1,2-dichloroethane, $[C_8mim]PF_6$ = 1-octyl-3-methylimidazolium hexafluorophosphate, ws = without additional solvent). [d] Cy conversion. [e] Homogeneous catalyst formed *in situ* identified as $[MoO(O_2)_2(L)]$. [f] Mo:Cy:TBHP = 1:113:172. [g] Mo:Cy:TBHP = 0.1:100:152.

After the catalytic reactions with TBHP or H_2O_2, work-up was performed to separate the solid and liquid phases, and the solids (**i**-Cat-oxidant) were characterised by ATR FT-IR spectroscopy and PXRD. The data indicated that the chemical and microstructural features of the undissolved solids **i**-Cat-TBHP (**i** = **1**-**5** or MoO_3) were unchanged relative to those for the original catalysts (Fig. S11 and S12 in the ESI†). On the other hand, for the undissolved solids **i**-Cat-H_2O_2 (***i*** = **1**-**4**), the data were consistent with the exclusive presence of the oxodiperoxo complex **5** (Fig. S13 and S14). Accordingly, the solid and liquid phases for (**1**-**4**)/Cy/H_2O_2 changed colour from white/colourless to yellow (complex **5** is yellow), while no comparable colour change was observed for (**1**-**4**)/Cy/TBHP. The catalytic activity of **5** for the Cy/H_2O_2 reaction (Fig. S10) indicates that this species contributes at least partially to the reaction kinetics of the systems (**1**-**4**)/Cy/H_2O_2. The catalytic performance of **5** resembles more closely that of the (pre)catalyst **1** than **2** and **3** (Fig. S10), which may be partly associated with the fact that the 2,2'-bipy/Mo ratio (*R*) in **5** and **1** is the same (equal to 1). There seems to be a relationship between catalytic activity and the ratio *R* in the (pre)catalyst, *i.e.* conversions at 6/24 h approximately follow the sequence *R* = 1 (**1**, **5**) < *R* = 0.67 (**3**) < *R* = 0.5 (**2**, **4**) < *R* = 0 (MoO_3). One cannot exclude the possibility that inorganic MoO_3-derived oxoperoxo species may be formed (together with **5**) from the precatalyst, and the amount of such species (which could be more active than **5**) may increase as the ratio *R* decreases. It is known that the reaction of MoO_3 with excess H_2O_2 can lead to oxodiperoxo species of the type $[MoO(O_2)_2(L)_2]$ and $[O\{MoO(O_2)_2(L)\}_2]^{2-}$ (L = H_2O, CH_3CN), which may contribute to the catalytic process.[28]

The catalytic performance of **2** was further investigated for the epoxidation of other cyclic and linear non-functionalised olefins, namely cyclododecene (Cy12), 1-octene (1C8) and *trans*-2-octene (2C8), under similar reaction conditions (Table 2). For these substrates the respective epoxides were always the only reaction products. The epoxidation of Cy12 gave 87 % yield of 1,2-epoxycyclododecane at 24 h. A comparison of the cyclic monoenes Cy12 and Cy indicates that the former is less reactive, which may be partly due to steric effects associated with the larger Cy12 molecules. On the other hand, a comparison of the linear monoenes 1C8 and 2C8 indicates that the latter is more reactive, which may be partly due to electronic effects favouring the epoxidation of internal C=C bonds in relation to that of terminal ones. These results are consistent with the literature in that the reaction mechanism of olefin epoxidation in the presence of molybdenum compounds may involve an O-atom transfer step where an electrophilic oxidising species (formed via reaction of the oxidant with the molybdenum catalyst) attacks the olefin.[21b,29] Overall, these results suggest that **2** is active for the epoxidation of cyclic and linear olefins, and may lead to high regioselectivity towards more substituted C=C bonds.

The hybrid **2** was further explored for the epoxidation of the biomass-derived olefins DL-limonene (Lim), α-pinene (Pin) and methyl oleate (Ole). The major sources of these compounds are citrus peel for Lim, turpentine (a byproduct of the wood pulp industry) for Pin, and vegetable oils for Ole. The corresponding epoxides, 1,2-epoxy-*p*-menth-8-ene (1,2-LimO), α-pinene oxide (PinO) and methyl 9,10-epoxyoctadecanoate (OleO), have a broad range of potential uses, e.g. as intermediates for the synthesis of perfumes, flavours, pharmaceuticals and bio-polymers.[30]

The catalytic epoxidation of Lim gave 1,2-LimO as the main product in 79 % yield at 24 h (Table 2), revealing a high regioselectivity towards epoxidation at the internal and more electron-rich endocyclic double bond. These results are comparable or superior to those reported for other polymeric oxomolybdenum compounds bearing pyridine-containing ligands (71-86 % yield).[23,25,27,31] Besides 1,2-LimO, 1,2:8,9-diepoxy-*p*-menthane and limonene diol were formed in 7 and 2 % yield, respectively. Increasing the TBHP:Lim molar ratio from 1.5 to 2 still led to 1,2-LimO as the main product (79 % yield at

24 h), further demonstrating the pronounced regioselectivity in favour of internal C=C bonds.

Table 2 Epoxidation of olefins with TBHP in the presence of $[Mo_2O_6(2,2'\text{-bipy})]$ (**2**).[a]

Substrate	Conv. (%)[b]	Epoxide	Sel. (%)[b]	TOF[c]
Cy	72/96	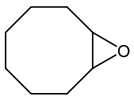	100/100	288
1C8	9/32	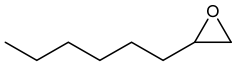	100/100	0
2C8	30/71	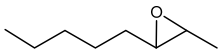	100/100	30
Cy12	41/87	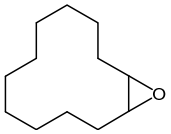	100/100	70
Lim	63/88	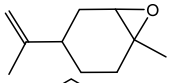	96/90	130
Pin	29/37	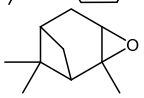	54/50	80
Ole	25/57	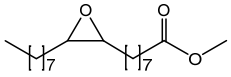	100/100	50

[a] Reaction conditions: Mo:TBHP:Olefin = 1:100:150, 55 °C. [b] Olefin conversion and epoxide selectivity at 6 h /24 h. [c] Turnover frequency (mol mol_{Mo}^{-1} h^{-1}).

The reaction of Pin gave PinO as the main product in 19 % yield at 24 h (Table 2). Other products included campholenic aldehyde (CPA), *trans*-pinocarveol (PCV) and *iso*-pinocamphone (IPC), formed in up to 9 % total yield. The formation of PinO rearrangement products like CPA and IPC is favoured in the presence of Lewis acid catalysts.[32] CPA is the most industrially important, being useful as an aroma chemical or as an intermediate in the synthesis other aromas (e.g. sandalwood-like fragrances) and some drugs.[33] IPC is one of the main components of Hyssop essential oil, which stimulates digestion, has expectorate properties, and antibacterial/fungal activity.[34]

The epoxidation of Ole gave mainly OleO, formed in 57 % yield at 24 h (Table 2). This performance compares favourably with that reported in the literature for the polymeric compound $[MoO_3(pbim)]$, which led to 42 % OleO yield at 69 % conversion (70 °C, 24 h).[27] Under comparable reaction conditions, $[(CH_3)_2NH_2][MoO_3(Hbpdc)]$ (H_2bpdc = 2,2'-bipyridine-5,5'-dicarboxylic acid), $[Mo_2O_6(pent\text{-}pzpy)]$ and $[Mo_8O_{22}(OH)_4(di\text{-}t\text{Bu-}bipy)_4]$ led to 77-92 % OleO yield at 77-94 % conversion (6-24 h).[25,31]

Conclusions

The study of the (hydro)thermal stability of the chainlike hybrid material $[MoO_3(2,2'\text{-bipy})]$ (**1**) has provided new syntheses of the related compounds $[Mo_2O_6(2,2'\text{-bipy})]$ (**2**) and $[Mo_3O_9(2,2'\text{-bipy})_2]$ (**3**) with yields that are superior to those obtained by hydrothermal methods using the free ligand 2,2'-bipy and simple molydate salts as starting materials. It is remarkable that the thermal removal of 2,2'-bipy from **1**, in the presence or absence of water, can be achieved selectively and in a stoichiometric fashion, with retention of the 1D molybdenum oxide chain structure, to give **2** and **3**. Compounds **1**-**3** belong to the $[(MoO_3)_m(2,2'\text{-bipyridine})_n]$ family of hybrid materials and provide an interesting opportunity to study the effect of the organic ligand ordering and distribution on the materials' properties. In the present work it has been shown that the ratio *m*/*n* influences catalytic performance for the epoxidation of olefins using hydroperoxide oxidants, with compound **2** leading to the best results. Under the reaction conditions used, the hybrid acts as a precatalyst for active species formed *in situ*, which promote high selectivities in the epoxidation of a variety of olefins. The hybrid phase **2** may therefore be a better oxidation (pre)catalyst than **1**, which has already demonstrated interesting behaviour when applied for the oxidation of other substrates such as sulfides and amines.

Conflicts of interest

There are no conflicts to declare.

Acknowledgements

This work was carried out with the support of CICECO - Aveiro Institute of Materials - POCI-01-0145-FEDER-007679 (FCT Ref. UID/CTM/50011/2013) and the CENTRO 2020 Regional Operational Programme (Project CENTRO-01-0145-FEDER-028031), co-financed by national funds through the FCT/MEC and the European Union through the European Regional Development Fund under the Portugal 2020 Partnership Agreement. The FCT and the European Union are acknowledged for a Ph.D. grant to L.S.N. (PD/BD/109666/2015), and post-doctoral grants to S.M.B. (SFRH/BPD/108845/2015) and A.C.G. (SFRH/BPD/108541/2015), co-funded by MCTES and the European Social Fund through the program POPH of QREN.

Notes and references

1 *(a)* I. A. de Castro, R. S. Datta, J. Z. Ou, A. Castellanos-Gomez, S. Sriram, T. Daeneke and K. Kalantar-zadeh, *Adv. Mater.*, 2017, **29**, 1701619; *(b)* B. Balendhran, S. Walia, H. Nili, J. Z. Ou, S. Zhuiykov, R. B. Kaner, S. Sriram, M. Bhaskaran and K. Kalantar-zadeh, *Adv. Funct. Mater.*, 2013, **23**, 3952-3970.

2 *(a)* Q. Huang, S. Hu, J. Zhuang and X. Wang, *Chem. Eur. J.*, 2012, **26**, 15283-15287; *(b)* M. Greenblatt, *Chem Rev.*, 1988, **88**, 31-53.

3 *(a)* A. Borgschulte, O. Sambalova, R. Delmelle, S. Jenatsch, R. Hany and F. Nüesch, *Sci. Rep.*, 2017, **7**, 40761; *(b)* B. Braïda, S. Adams and E. Canadell, *Chem. Mater.*, 2005, **17**, 5957-5969; *(c)* X. K. Hu, Y. T. Qian, Z. T. Song, J. R. Huang, R. Cao and J. Q. Xiao, *Chem. Mater.*, 2008, **20**, 1527-1533.

4 R. Schöllhorn, T. Schulte-Nölle and G. Steinhoff, *J. Less-Common Met.*, 1980, **71**, 71-78.

5 J. W. Johnson, A. J. Jacobson, S. M. Rich and J. F. Brody, *J. Am. Chem. Soc.*, 1981, **103**, 5246-5247.

6 *(a)* P. J. Hagrman, D. Hagrman and J. Zubieta, *Angew. Chem. Int. Ed.*, 1999, **38**, 2638-2684; *(b)* A. B. Lysenko, G. A. Senchyk,

J. Lincke, D. Lässig, A. A. Fokin, E. D. Butova, P. R. Schreiner, H. Krautscheid and K. V. Domasevitch, *Dalton Trans.*, 2010, **39**, 4223-4231; *(c)* M. Vougo-Zanda, X. Wang and A. J. Jacobson, *Inorg. Chem.*, 2007, **46**, 8819-8824.
7 P. J. Hagrman, R. L. LaDuca, Jr., H.-J. Koo, R. Rarig, Jr., R. C. Haushalter, M.-H. Whangbo and J. Zubieta, *Inorg. Chem.*, 2000, **39**, 4311-4317.
8 *(a)* X. Zhang, M. Hejazi, S. J. Thiagarajan, W. R. Woerner, D. Banerjee, T. J. Emge, W. Xu, S. J. Teat, Q. Gong, A. Safari, R. Yang, J. B. Parise and J. Li, *J. Am. Chem. Soc.*, 2013, **135**, 17401-17407; *(b)* B. Yan, Y. Xu, N. K. Goh and L. S. Chia, *Chem. Commun.*, 2000, 2169-2170.
9 Y. Xu, J. Lu and N. K. Goh, *J. Mater. Chem.*, 1999, **9**, 1599-1602.
10 *(a)* J. Chuang, W. Ouellette, J. Zubieta, *Inorg. Chim Acta,* 2008, **361**, 2357-2364; *(b)* T. R. Amarante, P. Neves, A. A. Valente, F. A. A. Paz, M. Pillinger and I. S. Gonçalves, *J. Catal.*, 2016, **340**, 354-367.
11 S. V. Chong, I. Udin and J. L. Tallon, *Mater. Lett.,* 2017, **204**, 141-144.
12 A. B. Lysenko, G. A. Senchyk, K. V. Domasevitch, J. Hauser, D. Fuhrmann, M. Kobalz, H. Krautscheid, P. Neves, A. A. Valente and I. S. Gonçalves, *Inorg. Chem.,* 2015, **54**, 8327–8338.
13 *(a)* P. J. Zapf, R. C. Haushalter, J. Zubieta, *Chem. Mater.*, 1997, **9**, 2019-2024; *(b)* T. R. Amarante, M. M. Antunes, A. A. Valente, F. A. A. Paz, M. Pillinger and I. S. Gonçalves, *Inorg. Chem.*, 2015, **54**, 9690-9703; *(c)* J. Kim, W. T. Lim and B. K. Koo, *Inorg. Chim.* Acta, 2007, **360**, 2187-2191.
14 *(a)* T. R. Amarante, P. Neves, A. C. Coelho, S. Gago, A. A. Valente, F. A. A. Paz, M. Pillinger and I. S. Gonçalves, *Organometallics*, 2010, **29**, 883−892; *(b)* M. Abrantes, T. R. Amarante, M. M. Antunes, S. Gago, F. A. A. Paz, I. Margiolaki, A. E. Rodrigues, M. Pillinger, A. A. Valente and I. S. Gonçalves, *Inorg. Chem.*, 2010, **49**, 6865-6873; *(c)* T. R. Amarante, P. Neves, A. C. Gomes, M. M. Nolasco, P. Ribeiro-Claro, A. C. Coelho, A. A. Valente, F. A. A. Paz, S. Smeets, L. B. McCusker, M. Pillinger and I. S. Gonçalves, *Inorg. Chem.*, 2014, **53**, 2652−2665.
15 I. Tosi, C. Vurchio, M. Abrantes, I. S. Gonçalves, M. Pillinger, F. Cavani, F. M. Cordero and A. Brandi, *Catal. Commun.*, 2018, **103**, 60-64.
16 F. E. Kühn, M. Groarke, É. Bencze, E. Herdtweck, A. Prazeres, A. M. Santos, M. J. Calhorda, C. C. Romão, I. S. Gonçalves, A. D. Lopes and M. Pillinger, *Chem. Eur. J.*, 2002, **8**, 2370–2383.
17 *(a)* M. C. Chakravorti, S. Ganguly and M. Bhattacharjee, *Polyhedron*, 1993, **12**, 55-58; *(b)* C. A. Gamelas, A. C. Gomes, S. M. Bruno, F. A. A. Paz, A. A. Valente, M. Pillinger, C. C. Romão and I. S. Gonçalves, *Dalton Trans.*, 2012, **41**, 3474–3484.
18 C. F. Macrae, I. J. Bruno, J. A. Chisholm, P. R. Edgington, P. McCabe, E. Pidcock, L. Rodriguez-Monge, R. Taylor, J. van de Streek and P. A. Wood, *J. Appl. Crystallogr.*, 2008, **41**, 466-470.
19 D. Li, B. H. O'Connor and H. Sitepu, *J. Appl. Crystallogr.*, 2005, **38**, 158-167.
20 J. Twu, Y.-Y. Yu, C.-W. Tang, G.-J. Wang and K.-H. Chen, *Appl. Spectrosc.*, 1999, **53**, 1083-1086.
21 *(a)* L. F. Veiros, Â. Prazeres, P. J. Costa, C. C. Romão, F. E. Kühn and M. J. Calhorda, *Dalton Trans.*, 2006, 1383-1389; *(b)* A. Comas-Vives, A. Lledós and R. Poli, *Chem. Eur. J.*, 2010, **16**, 2147-2158.
22 M. Herbert, F. Montilla, E. Álvarez and A. Galindo, *Dalton Trans.*, 2012, **41**, 6942-6956.
23 T. R. Amarante, P. Neves, F. A. A. Paz, M. Pillinger, A. A. Valente and I. S. Gonçalves, *Inorg. Chem. Commun.,* 2012, **20**, 147-152.
24 P. Neves, T. R. Amarante, A. C. Gomes, A. C. Coelho, S. Gago, M. Pillinger, I. S. Gonçalves, C. M. Silva and A. A. Valente, *Appl. Catal. A: Gen.*, 2011, **395**, 71-77.
25 T. R. Amarante, P. Neves, F. A. A. Paz, A. A. Valente, M. Pillinger and I. S. Gonçalves, *Dalton Trans.*, 2014, **43**, 6059-6069.
26 T. R. Amarante, A. C. Gomes, P. Neves, F. A. A. Paz, A. A. Valente, M. Pillinger and I. S. Gonçalves, *Inorg. Chem. Commun.*, 2013, **32**, 59-63.
27 P. Neves, L. S. Nogueira, A. C. Gomes, T. S. M. Oliveira, A. D. Lopes, A. A. Valente, I. S. Gonçalves and M. Pillinger, *Eur. J. Inorg. Chem.*, 2017, 2617-2627.
28 J.-Y. Piquemal, E. Briot and J.-M. Brégeault, *Dalton Trans.*, 2013, **42**, 29-45.
29 *(a)* N. Grover, M. Drees and F. E. Kühn, *J. Catal.*, 2015, **329**, 269-285; *(b)* M. J. Calhorda and P. J. Costa, *Curr. Org. Chem.*, 2012, **16**, 65-72; *(c)* P. J. Costa, M. J. Calhorda and F. E. Kühn, *Organometallics*, 2010, **29**, 303-311.
30 *(a)* M. Golets, S. Ajaikumar and J.-P. Mikkola, *Chem. Rev.*, 2015, **115**, 3141-3169; *(b)* A. Corma, S. Iborra and A. Velty, *Chem. Rev.*, 2007, **107**, 2411-2502; *(c)* P. Mäki-Arvela, B. Holmbom, T. Salmi and D. Y. Murzin, *Catal. Rev.*, 2007, **49**, 197-340; *(d)* S. M. Danov, O. A. Kazantsev, A. L. Esipovich, A. S. Belousov, A. E. Rogozhin, E. A. Kanakov, *Catal. Sci. Technol.*, 2017, **7**, 3659-3675; *(e)* A. F. Lee, J. A. Bennet, J. C. Manayil and K. Wilson, Chem. Soc. Rev., 2014, **43**, 7887-7916; *(f)* A. Köckritz and A. Martin, *Eur. J. Lipid Sci. Technol.*, 2008, **110**, 812-824.
31 *(a)* T. R. Amarante, P. Neves, C. Tomé, M. Abrantes, A. A. Valente, F. A. A. Paz, M. Pillinger and I. S. Gonçalves, *Inorg. Chem.*, 2012, **51**, 3666-3676; *(b)* T. R. Amarante, P. Neves, A. A. Valente, F. A. A. Paz, A. N. Fitch, M. Pillinger and I. S. Gonçalves, *Inorg. Chem.*, 2013, **52**, 4618-4628.
32 G. Neri, G. Rizzo, A. Pistone, L. De Luca, A. Donato, M. G. Musolino and R. Pietropaolo, *Appl. Catal. A: Gen.*, 2007, **325**, 25-33.
33 *(a)* C. Brocke, M. Eh and A. Finke, *Chem. Biodivers.*, 2008, **5**, 1000-1010; *(b)* B. J. Kane, G. P. Sanders, J. W. Snow and M. B. Erman, U. S. Patent 169343 (2002).
34 G. Zawislak, *J. Essent. Oil Bear. Pl.*, 2016, **19**, 699-705.